

**Carrier-envelope phase mapping in laser-induced electron diffraction**Henning Geiseler,<sup>1,\*</sup> Nobuhisa Ishii,<sup>1</sup> Keisuke Kaneshima,<sup>1</sup> Florian Geier,<sup>1</sup> Teruto Kanai,<sup>1</sup> Oleg I. Tolstikhin,<sup>2</sup>  
Toru Morishita,<sup>3</sup> and Jiro Itatani<sup>1</sup><sup>1</sup>*The Institute for Solid State Physics, The University of Tokyo, 5-1-5 Kashiwanoha, Kashiwa, Chiba 277-8581, Japan*<sup>2</sup>*Moscow Institute of Physics and Technology, Dolgoprudny 141700, Russia*<sup>3</sup>*Institute for Advanced Science, The University of Electro-communications, 1-5-1 Chofu-ga-oka, Chofu-shi, Tokyo 182-8585, Japan*

(Received 2 April 2015; revised manuscript received 16 June 2016; published 19 September 2016)

We present laser-induced electron diffraction measurements of elastic differential scattering cross sections (DCSs) of a photoelectron on the parent ion for argon, krypton, and xenon, using waveform-controlled few-cycle pulses. Considering only cutoff electrons and employing the adiabatic theory for the analysis enables us to eliminate ambiguities in extracting the DCSs from experimental spectra. Contrary to previous works, which mainly focused on the angular dependence of the DCS, our method allows us to extract also its dependence on the scattering momentum. In the case of xenon, we demonstrate how this method can be used to obtain the complete angular and momentum dependence of the DCS in a range of these variables determined by the pulse. The obtained results are compared to theoretical calculations based on the single-active-electron approximation, which shows a high level of agreement. Further investigations may provide opportunities to study multielectron effects when more advanced theoretical models become available.

DOI: [10.1103/PhysRevA.94.033417](https://doi.org/10.1103/PhysRevA.94.033417)**I. INTRODUCTION**

It is a long-standing goal in optical science to directly image molecules undergoing structural transformations on their natural length and time scales. Ultrafast laser systems nowadays routinely achieve sufficiently short pulse durations, but since they typically operate near the visible spectrum, the achievable spatial resolution, of the order of 100 nm, is too rough. Molecular structures of the order of 0.1 nm can routinely be resolved using electron or x-ray diffraction, but here, even with sophisticated techniques, the temporal resolution is still orders of magnitude too low [1]. Only recently, technological progress in free-electron lasers made available ultrashort, highly energetic x-ray pulses that can be used for dynamic molecular imaging [2], but due to the sheer size and cost of these facilities they are not widely available for a broad application to research.

A few years ago, an alternative approach emerged with laser-induced electron diffraction (LIED) [3], which relies on photoionization in intense low-frequency laser fields. The ionization dynamics in this regime can be qualitatively interpreted by an instructive semiclassical model [4], allowing LIED to be described as self-imaging of the target by laser-field-accelerated photoelectrons. Since this rescattering process is intrinsically linked to the driving pulses, the atomic-scale temporal resolution of ultrafast lasers can be preserved, and LIED offers the potential for spatiotemporal resolution necessary for dynamic molecular imaging, using only tabletop-scale experimental equipment [5,6].

A pivotal achievement in the development of LIED techniques was the theoretical discovery of factorization of strong-field photoelectron momentum distributions (PEMDs) in the region of near-backward rescattering. It was first recognized from numerical calculations [7] and then derived by different analytical methods [8–10] that PEMDs can be factorized into the field-free differential scattering cross

section (DCS) of a photoelectron on the parent ion and a returning electron wave packet (RWP). This result allows us to experimentally extract the angular dependence of the DCS at a fixed scattering momentum, which was initially demonstrated for the noble gases [11,12]. Strictly speaking, the factorization holds only for the cutoff, that is, the most energetic of rescattered photoelectrons. But numerical studies showed that in certain cases PEMDs at lower momenta also could be approximated using this description [13], which was demonstrated experimentally for atoms [14] and small molecules [15,16]. The extracted DCSs encode the target structural information, which can thus be recovered [17,18]. However, this approach suffers from important limitations, as the assumption of factorization of PEMDs at intermediate momenta introduces an error. Moreover, due to experimental volume effects that occur in this regime, the normalization of angular distributions of the DCS at different momenta is extremely challenging [19]. So far, theoretical DCSs were used for normalization, thus actual experimental insight was provided only into the angular dependence of the DCS.

In this paper, we demonstrate LIED using few-cycle pulses with a well-defined carrier-envelope phase (CEP) and extract the DCSs of noble gases. Our main results are twofold. Experimentally, we demonstrate a new technique that maps the CEP to the scattering momentum, allowing us to access the complete DCS, including its scattering momentum dependence. Theoretically, we apply the adiabatic theory [20], whose solid foundations were confirmed in Refs. [21] and [22], to the extraction procedure, removing approximations and ambiguities of previous approaches. The key feature of our method is that we consider only cutoff electrons, so that the factorization is well justified. For few-cycle pulses, the cutoff position depends sensitively on the CEP [23], which enables us to probe an extended momentum range.

**II. THE ADIABATIC THEORY**

We assume that the ionizing pulse is linearly polarized along the  $z$  axis, and the electric field is  $\mathbf{F}(t) = F(t)\mathbf{e}_z$ . Within the

\*geiseler@issp.u-tokyo.ac.jp

simple asymptotics of the adiabatic theory [20], the moments of ionization  $t_i$  and rescattering  $t_r$  for a given photoelectron momentum  $\mathbf{k} = (k_\perp, k_z)$  are defined by the equations (atomic units are used throughout, unless otherwise noted)

$$(t_r - t_i)v(t_i) = \int_{t_i}^{t_r} v(t) dt, \quad (1a)$$

$$[v(t_r) - v(t_i)]^2 = k_\perp^2 + [k_z - v_\infty + v(t_r)]^2, \quad (1b)$$

where  $v(t) = -\int_{-\infty}^t F(t') dt'$  and  $v_\infty = v(\infty)$ . The incident momentum and scattering angle for the rescattering event are then given by  $\mathbf{p} = u_f \mathbf{e}_z$  and  $\theta = \arccos([k_z - v_\infty + v(t_r)]/u_f)$ , respectively, where  $u_f = v(t_r) - v(t_i)$ . Equations (1) may have multiple solutions corresponding to different rescattering trajectories with the same final momentum  $\mathbf{k}$ . The number of solutions depends on  $\mathbf{k}$ . For any given pulse shape defined by the function  $F(t)$ , there exists a cutoff line in the  $(k_\perp, k_z)$  plane outside which there are no solutions, and hence the rescattering part of the PEMD rapidly becomes 0. Inside the line, in its vicinity, Eqs. (1) have two solutions, which correspond to long and short rescattering trajectories originating from the same half-cycle [10]. This line is a caustic where the two trajectories coalesce. This happens when the solutions of Eqs. (1) satisfy an additional equation,

$$S_r'' = -F(t_r)[k_z - v_\infty + v(t_i)] + u_f^2/(t_r - t_i) = 0, \quad (2)$$

where  $S_r$  is the corresponding classical action [20]. It is convenient to parametrize the caustic by the scattering angle  $\theta$  for the coalesced trajectories, that is, to consider  $t_i$  and  $t_r$  satisfying Eqs. (1) and (2), and hence  $u_f$ , as functions of  $\theta$ . Then the position of the caustic  $\mathbf{k}(\theta)$  in the  $(k_\perp, k_z)$  plane is defined by

$$k_\perp(\theta) = |u_f(\theta)| \sin \theta, \quad (3a)$$

$$k_z(\theta) = u_f(\theta) \cos \theta - v(t_r(\theta)) + v_\infty. \quad (3b)$$

Using the results of Ref. [20], we obtain that along the caustic the PEMD takes the factorized form

$$P(\mathbf{k}(\theta)) = |f(p, \theta)|^2 W(\theta), \quad (4)$$

where  $f(p, \theta)$  is the scattering amplitude defining the DCS  $d\sigma/d\Omega = |f(p, \theta)|^2$ ,  $p = |u_f(\theta)|$  is the scattering momentum, and the factor  $W(\theta)$  represents the RWP. In the weak-field limit [24] it is given by

$$W(\theta) = 16\pi^3 \text{Ai}^2(0) \left| \frac{2}{S_r'''} \right|^{2/3} \frac{\kappa \Gamma(t_i)}{(t_r - t_i)^3 F^2(t_i)} \times \exp \left[ -\int_{-\infty}^{t_i} \Gamma(t) dt \right], \quad (5)$$

where

$$S_r''' = u_f \left[ 2\dot{F}(t_r) \sin^2(\theta/2) - \frac{2F(t_r) \cos^2(\theta/2)}{t_r - t_i} - \dot{F}(t_i) \left( \frac{dt_i}{dt_r} \right)^2 - F(t_i) \frac{d^2 t_i}{dt_r^2} \right]. \quad (6)$$

Here  $\text{Ai}(z)$  is the Airy function,  $\kappa = \sqrt{2I_p}$ , with  $I_p$  being the field-free ionization potential,  $\Gamma(t)$  is the tunneling ionization rate at the instantaneous field strength  $|F(t)|$ , and all the quantities should be calculated at the caustic.

Equation (4) has the form of the factorization formula proposed in Ref. [7]. Our main achievement here is that we have obtained the explicit analytic expression, (5), for the RWP. It should be emphasized that contrary to the assumptions in earlier works [7, 12, 14–19], the RWP does exhibit a significant dependence on  $\theta$ . Another difference is that the caustic, where the factorization holds, deviates particularly towards small  $\theta$  from the simple circular approximation used in these studies. These differences affect the extracted DCSs.

### III. CEP MAPPING EXPERIMENTS

Experimentally it has been established that the optimal compromise for the implementation of LIED is using infrared wavelengths, as with longer wavelengths the rescattering probability becomes too low, while with shorter wavelengths it is difficult to reach sufficiently high scattering energies [25]. Therefore, pulses centered at 1.6  $\mu\text{m}$  from our optical parametric chirped-pulse amplification system [26, 27] are ideally suited. The broad amplification bandwidth of the employed BiBO crystal allows us to maintain an octave-spanning spectrum of the amplified pulses and to compress these to durations around 10 fs (full width at half-maximum of the intensity), which corresponds to less than two optical cycles. For the proposed experimental approach, this is essential in order to isolate a single half-cycle cutoff (HCO [28]) spanning a broad spectral range. The total pulse energy was 550  $\mu\text{J}$ , but it could be attenuated by a variable iris in the beam path to adjust the peak intensity at the focus. The CEP was controlled via an acousto-optic programmable dispersive filter with an accuracy better than 250 mrad, and the system has been demonstrated to offer long-term stability of both the CEP and the pulse energy for more than 45 h [29]. This method of CEP control ensures that the spatial and temporal properties of the pulse envelope remain unaffected when the CEP is changed. To acquire photoelectron spectra, the pulses were loosely focused into a vacuum chamber by a concave mirror with a focal length of 37.5 cm, ionizing atoms of a sample gas in an effusive beam. The loose focusing geometry is necessary in order to mitigate Gouy phase effects, which would otherwise obfuscate the CEP sensitivity. The energy of generated photoelectrons was measured using a time-of-flight spectrometer with a 48-cm-long field-free flight tube. The polarization of the ionizing pulses relative to the spectrometer axis could be freely rotated by a half-wave plate in front of the focusing mirror.

First, we performed photoelectron measurements of argon, krypton, and xenon, respectively, along the laser polarization axis, thus detecting only electrons scattered at  $\theta = 180^\circ$ . The pulse energy was attenuated to the minimum value that still allowed us to acquire statistically meaningful data in a reasonable time (typically 10 h for a complete CEP scan with our 1-kHz light source). Due to the different ionization potentials, the pulse energy had to be set at different values for each gas species. The CEP was scanned in steps of  $0.1\pi$  rad, and the obtained spectral maps are shown in Fig. 1(a). The dependence of the cutoff on the CEP is prominently visible, and individual HCOs are easily identified. For visual reference, they are shown by black lines. The shape of these HCOs can be reproduced by Eq. (3b), fixing  $\theta = 180^\circ$  and scanning the CEP

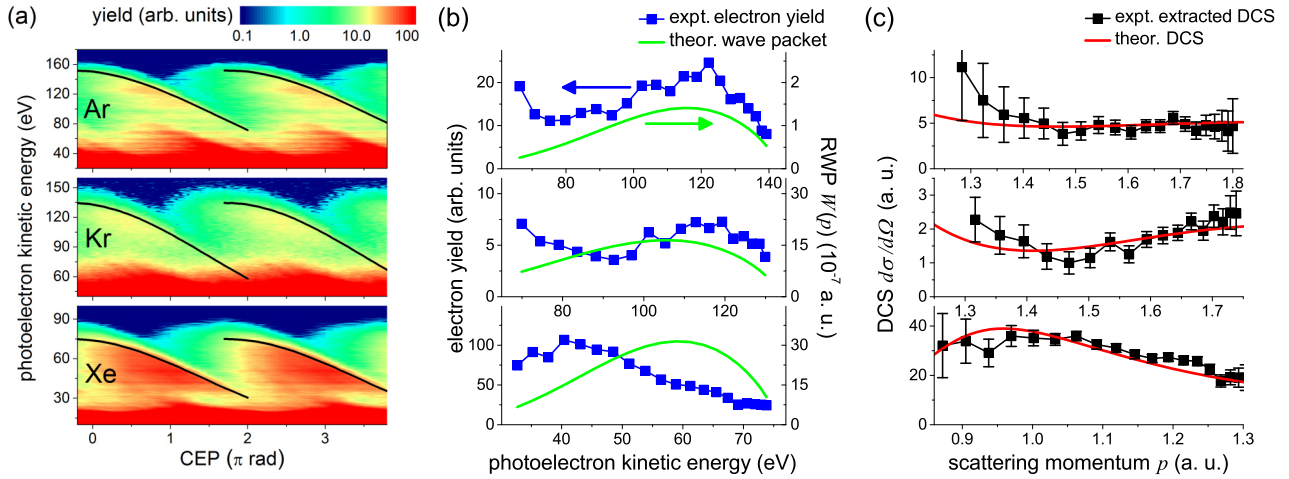


FIG. 1. (a) Photoelectron spectra as functions of the CEP for  $\theta = 180^\circ$  from argon, krypton, and xenon, respectively. HCOs are indicated by black lines. (b) Photoelectron yields obtained along these HCOs (blue squares) and RWPs calculated using Eq. (5) (green lines). (c) Experimentally extracted (black squares) and theoretically calculated (red lines) DCSs as functions of  $p$ .

of a pulse  $F(t)$  with an assumed Gaussian envelope. Fitting the pulse parameters so that the HCOs match the experimental spectra, the absolute CEP in the experiment can be reliably calibrated [30]. Furthermore, the maximum cutoff energy allows us to infer the peak intensity present in the experiment, and the slope of the HCOs provides a sensitive measure for the actual pulse duration. In our experiments, we determined peak intensities of  $6.3$ ,  $5.5$ , and  $3.2 \times 10^{13}$  W/cm<sup>2</sup> for argon, krypton, and xenon, respectively. The pulse durations were 11.6, 10.6, and 11.0 fs, respectively.

To extract the DCSs, first we plot the photoelectron yields along the indicated HCOs for all three measurements in Fig. 1(b). According to Eq. (4), these yields are in a simple functional relation with the DCSs. Using the pulse parameters determined above, we therefore calculate the cutoff RWPs via Eq. (5) as functions of the scattering momentum along the respective HCOs, which is shown by green lines in Fig. 1(b). The RWPs exhibit a pronounced maximum when the CEP approaches  $1.0\pi$  rad, because at this CEP the  $t_i$  leading to cutoff electrons passes through the maximum of the pulse envelope, so that the instantaneous tunnel-ionization rate is highest. Dividing the experimental electron yields by the RWPs results in the DCSs for backscattering, where the values of  $p$  for each CEP step are found via Eqs. (1), and the results are shown in Fig. 1(c). For comparison we also show numerically calculated DCSs that were obtained by solving the time-independent Schrödinger equation in the single-active-electron (SAE) approximation, using a model potential that is adapted to reproduce the known energy levels of the respective ion species and the  $R$ -matrix propagation method. The theoretical DCSs fall largely within the margin of error of the experimental values, especially in the center of the probed momentum ranges. Towards the lower momentum edge (CEP approaching  $2.0\pi$  rad) deviations occur, because increasingly spurious low-energy direct electrons interfere with the measurement.

Adding angular resolution to the measurements, this concept can be extended to extract complete DCSs. We demonstrate this in the case of xenon by varying the polarization angle

relative to the spectrometer axis in steps of  $10^\circ$  in successive experiments. For a fixed CEP, the two-dimensional PEMD can thus be recovered, which is shown in Fig. 2(a) for selected CEP values. From each of the set of 21 PEMDs between 0 and  $2\pi$  rad, we extracted the angular distribution of the rescattered photoelectrons at the respective caustic. The caustic according to Eqs. (3) is indicated in each panel in Fig. 2(a). It can be

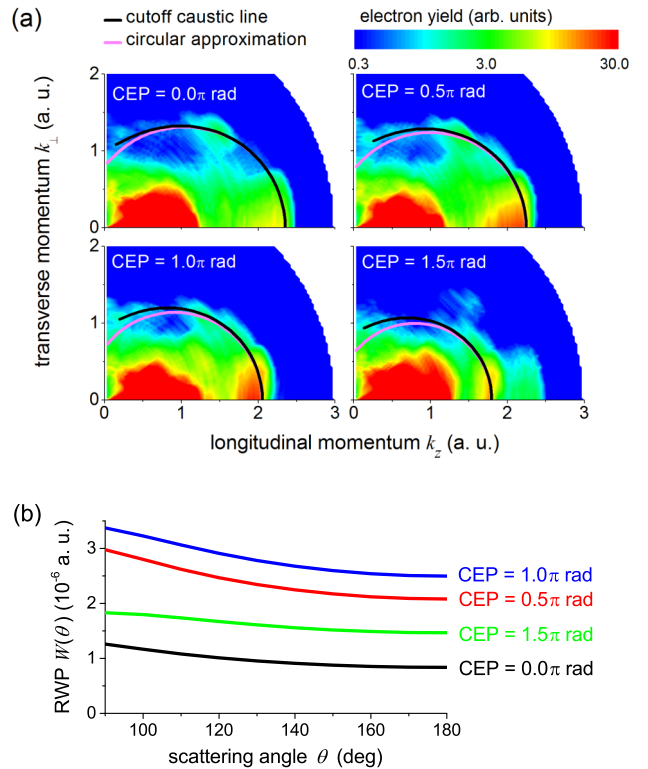


FIG. 2. (a) Two-dimensional PEMDs from xenon for different values of the CEP. Black lines show the position of the caustic, and magenta lines of the circular approximation, where  $p$  is constant. (b) Angular dependence of the RWP along the caustic, calculated by Eq. (5) for the CEP values in (a).

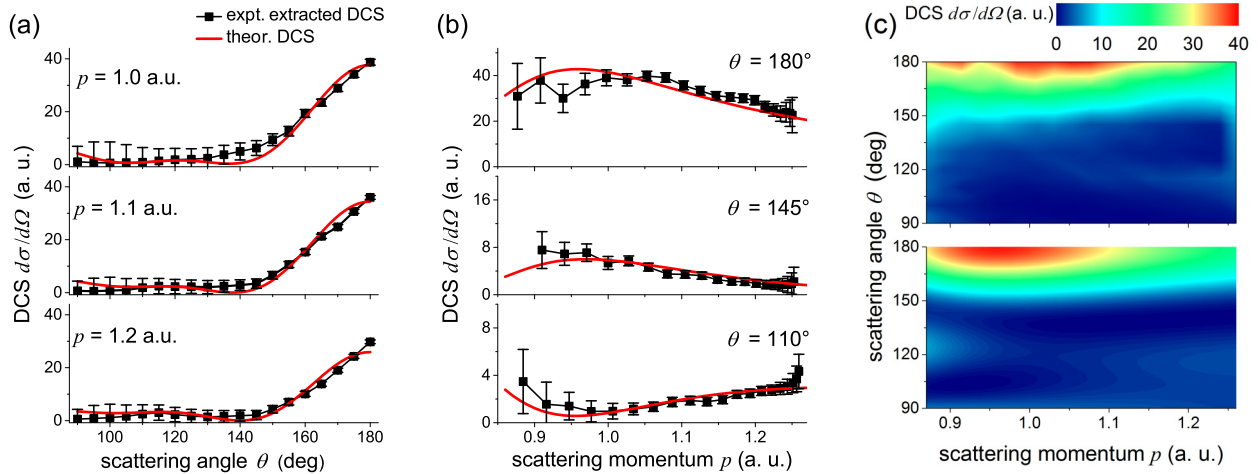


FIG. 3. (a) Angular dependence of the extracted and calculated DCS of xenon for selected  $p$  values. (b) Momentum dependence of the extracted and calculated DCS of xenon for selected  $\theta$  values. (c) Upper panel: Two-dimensional representation of the extracted DCS of xenon. Lower panel: Results of the SAE calculation for comparison.

seen that this caustic deviates significantly from the circular approximation when  $\theta$  is decreased below  $\approx 90^\circ$ . In the same way as the above experiment, the RWPs are calculated using Eq. (5) in order to extract the DCSs from cutoff electron yields. For the sample CEP values in Fig. 2(a) these RWPs are shown in Fig. 2(b). Besides a pronounced dependence on the CEP (i.e., the scattering momentum  $p$ ), they also depend significantly on the scattering angle  $\theta$ . Division again yields the DCSs, which can now be presented as a function of either  $\theta$  [shown in Fig. 3(a)] or  $p$  [shown in Fig. 3(b)]. The upper panel in Fig. 3(c) shows a combined representation as a color-coded plot. All results are compared to results of the SAE calculations and show very good agreement over the entire range, particularly towards  $\theta = 90^\circ$ , where previous works often yielded experimental values that were too high [11,12,14].

#### IV. CONCLUSIONS

In summary, we have demonstrated a method to use CEP-stable few-cycle pulses for LIED of noble gases, which allows us to map the CEP to the cutoff electron scattering momentum in a controlled way. We presented an analytically derived expression for the RWP based on the adiabatic theory, which

allows us to directly access the momentum dependence of the DCS from our experimental spectra, removing inaccuracies of previous approaches. For xenon, we also combined this method with angularly resolved LIED, to extract the complete DCS. Our results agree well with calculations based on the SAE approximation. In the future, the method might be refined using higher-repetition-rate light sources or advanced detection techniques, and it might be used to investigate electron correlation effects in the DCS, which are not yet incorporated into the theoretical models. We have demonstrated the technique using noble gases, but we expect that the same principles can also be applied to molecular targets and, thus, contribute to the development of methods for dynamic molecular imaging.

#### ACKNOWLEDGMENTS

We thank K. L. Ishikawa for helpful discussions. This research was supported in part by Grant-in-Aid for Scientific Research (S) No. 23226003 and Grant-in-Aid for Young Scientists (B) No. 25790063, from the Japan Society for the Promotion of Science. O.I.T. acknowledges support from the Ministry of Education and Science of Russia (State Assignment No. 3.679.2014/K). T.M. was supported in part by Grant-in-Aid for Scientific Research (C) No. 26400415 from the Japan Society for the Promotion of Science.

- 
- [1] A. Zewail, *Annu. Rev. Phys. Chem.* **57**, 65 (2006).  
 [2] A. Barty, J. Küpper, and H. N. Chapman, *Annu. Rev. Phys. Chem.* **64**, 415 (2013).  
 [3] M. Meckel, D. Comtois, D. Zeidler, A. Staudte, D. Pavičić, H. C. Bandulet, H. Pépin, J. C. Kieffer, R. Dörner, D. M. Villeneuve *et al.*, *Science* **320**, 1478 (2008).  
 [4] P. B. Corkum, *Phys. Rev. Lett.* **71**, 1994 (1993).  
 [5] C. Blaga, J. Xu, A. DiCiara, E. Sistrunk, K. Zhang, P. Agostini, T. A. Miller, L. DiMauro, and C. D. Lin, *Nature* **483**, 194 (2012).  
 [6] M. G. Pullen, B. Wolter, A. T. Le, M. Baudisch, M. Hemmer, A. Senfleben, C. D. Schröter, J. Ullrich, R. Moshhammer, C. D. Lin *et al.*, *Nat. Commun.* **6**, 7262 (2015).  
 [7] T. Morishita, A. T. Le, Z. Chen, and C. D. Lin, *Phys. Rev. Lett.* **100**, 013903 (2008).  
 [8] A. Čerkić, E. Hasović, D. B. Milošević, and W. Becker, *Phys. Rev. A* **79**, 033413 (2009).  
 [9] M. V. Frolov, N. L. Manakov, and A. F. Starace, *Phys. Rev. A* **79**, 033406 (2009).

- [10] O. I. Tolstikhin, T. Morishita, and S. Watanabe, *Phys. Rev. A* **81**, 033415 (2010).
- [11] M. Okunishi, T. Morishita, G. Prümper, K. Shimada, C. D. Lin, S. Watanabe, and K. Ueda, *Phys. Rev. Lett.* **100**, 143001 (2008).
- [12] D. Ray, B. Ulrich, I. Bocharova, C. Maharajan, P. Ranitovic, B. Gramkow, M. Magrakvelidze, S. De, I. V. Litvinyuk, A. T. Le *et al.*, *Phys. Rev. Lett.* **100**, 143002 (2008).
- [13] Z. Chen, A. T. Le, T. Morishita, and C. D. Lin, *Phys. Rev. A* **79**, 033409 (2009).
- [14] T. Morishita, M. Okunishi, K. Shimada, G. Prümper, Z. Chen, S. Watanabe, K. Ueda, and C. D. Lin, *J. Phys. B* **42**, 105205 (2009).
- [15] M. Okunishi, H. Niikura, R. R. Lucchese, T. Morishita, and K. Ueda, *Phys. Rev. Lett.* **106**, 063001 (2011).
- [16] C. Wang, M. Okunishi, R. R. Lucchese, T. Morishita, O. I. Tolstikhin, L. B. Madsen, K. Shimada, D. Ding, and K. Ueda, *J. Phys. B* **45**, 131001 (2012).
- [17] J. Xu, H. L. Zhou, Z. Chen, and C. D. Lin, *Phys. Rev. A* **79**, 052508 (2009).
- [18] T. Morishita, T. Umegaki, S. Watanabe, and C. D. Lin, *J. Phys.: Conf. Ser.* **194**, 012011 (2009).
- [19] M. Okunishi, R. R. Lucchese, T. Morishita, and K. Ueda, *J. Electron Spectrosc.* **195**, 313 (2014).
- [20] O. I. Tolstikhin and T. Morishita, *Phys. Rev. A* **86**, 043417 (2012).
- [21] M. Ohmi, O. I. Tolstikhin, and T. Morishita, *Phys. Rev. A* **92**, 043402 (2015).
- [22] Y. Zhou, O. I. Tolstikhin, and T. Morishita, *Phys. Rev. Lett.* **116**, 173001 (2016).
- [23] H. Geiseler, N. Ishii, K. Kaneshima, K. Kitano, T. Kanai, and J. Itatani, *J. Phys. B* **47**, 204011 (2014).
- [24] O. I. Tolstikhin, T. Morishita, and L. B. Madsen, *Phys. Rev. A* **84**, 053423 (2011).
- [25] J. Xu, C. Blaga, A. DiChiara, E. Sistrunk, K. Zhang, Z. Chen, A. T. Le, T. Morishita, C. D. Lin, P. Agostini *et al.*, *Phys. Rev. Lett.* **109**, 233002 (2012).
- [26] N. Ishii, K. Kaneshima, K. Kitano, T. Kanai, S. Watanabe, and J. Itatani, *Opt. Lett.* **37**, 4182 (2012).
- [27] N. Ishii, K. Kaneshima, T. Kanai, S. Watanabe, and J. Itatani, *J. Opt.* **17**, 094001 (2015).
- [28] C. A. Haworth, L. E. Chipperfield, J. S. Robinson, P. L. Knight, J. P. Marangos, and J. W. G. Tisch, *Nat. Phys.* **3**, 52 (2007).
- [29] H. Geiseler, N. Ishii, K. Kaneshima, T. Kanai, and J. Itatani, *Appl. Phys. B* **117**, 941 (2014).
- [30] S. Micheau, Z. Chen, A. T. Le, J. Rauschenberger, M. F. Kling, and C. D. Lin, *Phys. Rev. Lett.* **102**, 073001 (2009).